Target and energy dependence of intermittency and multifractality in interactions at cosmic ray energies

R. K. Shivpuri and Neeti Parashar
Department of Physics and Astrophysics, University of Delhi, Delhi - 110007, India
(Received 19 April 1993; revised manuscript received 23 August 1993)

We present here detailed results on intermittency and multifractality in interactions at cosmic ray energies. Intermittency has been investigated in terms of the scaled factorial moments for nucleon and AgBr targets. The intermittency signal has been found to be more for the nucleon as compared to AgBr targets. The primary energy dependence of intermittency has been studied for interactions with primary energies less than 1 TeV and greater than 1 TeV. With increase in primary energy, the intermittency signal decreases. The power-law behavior of the G_q moments suggests a multifractal behavior. The spectrum $f(\alpha_q)$ of the rapidity density index α_q has been determined for nucleon and AgBr targets and also for different primary energies and its behavior shows self-similarity. No evidence for a phase transition is indicated. The rescaled spectrum $\bar{f}(\bar{\alpha}_q)$ for nucleon and AgBr targets and for different primary energies has been investigated. The distributions show the universality of the multifractal structure for $q > 1$.

PACS number(s): 13.85.Tp, 13.85.Hd

I. INTRODUCTION

Ever since the observation of nonstatistical rapidity fluctuations in high-energy interactions, this subject has triggered intense experimental and theoretical investigations. The first event to have shown the existence of rapidity fluctuations was due to cosmic rays, observed by the JACEE Collaboration [1]. Bialas and Peschanski [2] were the first to investigate the power-law behavior of factorial moments of multiplicity fluctuations on the rapidity bin width. They called this phenomenon intermittency, the name being derived from turbulence in chaos [3]. The study of factorial moments offers a new way to understand the dynamics of the hadronization process. Experimental support for intermittent behavior was obtained from e^+e^- annihilation [4], hadron-hadron [5], hadron-nucleus [6], and nucleus-nucleus [6(a),7] interactions.

Although a number of experiments have reported observations of intermittent behavior of secondary particles at different primary energies, no attempt has been made to investigate the intermittency and multifractal characteristics of interactions at cosmic ray energies. We present here the first such study of fractal characteristics of interactions at ultrahigh energies.

Deterministic chaos in nonlinear physics has been well explained in terms of fractal measures [8]. Study of intermittent behavior in turbulent fluids has been done using the fractal dimension [9]. This has prompted exploration of intermittency in multiparticle production in terms of the multifractal formalism of fractal properties in multiparticle production processes. It has been suggested [10] that the fluctuation in rapidity has a nontrivial multifractal structure. The advantage of the multifractal analysis is that it allows the extension of our study to negative moments, whereas the factorial moments are defined for positive integral orders only. Carruthers and Minh [11] were the first to study the fractal dimensions in multiparticle production. Several authors [9,12] have suggested different approaches to study the fractal dimensions. However, Hwa [13] was the first to provide an attractive formalism based on G_q moments for investigating the multifractality.

The spectrum $f(\alpha_q)$ [13] of the rapidity density index α_q derived from the fractal G_q moments has been predicted to have interesting characteristics which reproduce the inhomogeneity of the rapidity distribution. The special function $f(\alpha_q)$ has described well the rapidity fluctuations in e^+e^- annihilations [14], $\bar{p}p$ collisions [15], π^-p and K^+p collisions [16], and μp and μd collisions [17].

In the present work, we present results on intermittency and multifractality in multiparticle production in nucleon-induced interactions at cosmic ray energies. Interactions with nucleon and AgBr targets have been studied separately to determine the target dependence of intermittency. Further, in order to study the dependence on primary energy, interactions were classified into categories having primary energies <1 TeV and >1 TeV. We have studied the factorial moments and the anomalous fractal dimension for both nucleon and AgBr targets at the above primary energies. The existence of a phase transition [18] in the various classes of interactions has been investigated. For the multifractal analysis, we have studied the G_q moments, the Renyi dimension, and the spectrum $f(\alpha_q)$ of scaling indices. The rescaled spectrum $\bar{f}(\bar{\alpha}_q)$ [19] has been determined to investigate the universality that unifies the multifractal structure for positive order of moments for different targets and primary energies.

II. THE DATA

The data used in the present work is from the ICEF Collaboration [20], which contains details of the events such as their shower and heavy track multiplicities, primary energy and $\ln\tan\theta$ of individual particles in the

events. Following the usual emulsion terminology [21], shower tracks are due to particles having velocities $\beta \geq 0.7$ ($\beta = v/c$) corresponding to ionization $I < 1.4 I_{\min}$, where $I_{\min}$ is the minimum ionization in the emulsion. The multiplicity of shower and heavy tracks is called N_s and N_h, respectively. In order to correct for the leading particle effect, the primary energy was calculated using Castagnoli *et al.*'s formula [22], after eliminating the contribution of smallest angle track. This procedure [23] leads to a better estimate of the primary energy (E_p).

It has been shown [21] that N_h can be used as a monitor to indicate the number of nucleons taking part in the interaction. Hence the value of N_h can be used to determine the type of target involved in the interaction. Events with $N_h = 0,1$ are mostly due to the nucleon while those with $N_h \geq 9$ are unambiguously due to AgBr targets. In order to study the target dependence, we have classified the events due to nucleon and AgBr targets. Events with primary energy $E_p < 1$ TeV and $E_p > 1$ TeV have been separately analyzed for investigating the primary energy dependence of various parameters.

A total of 440 events were considered in the present work. The number of events belonging to nucleon and AgBr targets were 42 and 137, respectively. The number of events with $E_p < 1$ TeV and $E_p > 1$ TeV were 315 and 125, respectively. In the present analysis, we have not considered events with $N_s \leq 10$. For such events the number of particles in any bin is very small and it becomes difficult to disentangle the nonstatistical from the statistical fluctuations. We have calculated the pseudorapidity (η) of the shower particles, which is given by, $\eta = -\ln(\tan\theta/2)$, where θ is the lab angle of the shower particle. Figure 1 shows the η distribution of the secondary particles for some events.

Presently, only cosmic rays provide primary energies > 1 TeV for fixed targets. The number of events with $E_p > 1$ TeV and for AgBr targets (excluding $N_s \leq 10$) is 30. We show in Table I the event type, primary energy, and pseudorapidity values of the secondary particles for these events. The usual nonmenclature [20] of $N_h + N_s$ primary is followed for designating each event, where the first term shows the value of N_h, the second number designates N_s, and the primary denotes the type of incident particle.

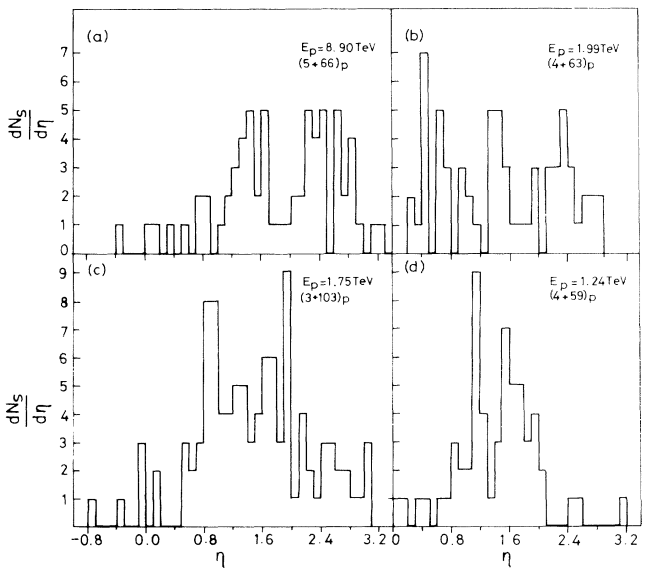

FIG. 1. Pseudorapidity (η) distributions for various high multiplicity interactions at cosmic ray energies.

III. THE INTERMITTENCY

In order to understand quantitatively the intermittent behavior of interactions, Bialas and Peschanski [2] suggested the usage of scaled factorial moments. Let the pseudorapidity interval $\Delta\eta$ of the interactions be divided into M bins of size $\delta\eta = \Delta\eta/M$. For events of varying multiplicity, the qth-order moment is defined [2] as

$$\langle F_q \rangle = \frac{1}{N_{\rm ev}} \sum_{N_{\rm ev}} M^{q-1} \sum_{m=1}^{M} \frac{k_m(k_m-1)\cdots(k_m-q+1)}{\langle N \rangle^q} , \tag{1}$$

where k_m is the number of particles in the mth bin of a single event, $\langle N \rangle$ is the average particle multiplicity in the pseudorapidity range $\Delta\eta$, and $N_{\rm ev}$ denotes the number of events. It was shown [2] that the scaled factorial moments averaged over many events are equal to the scaled moments of the parent probability distributions of particles in phase space and the values of $\langle F_q \rangle$ do not show any dependence on $\delta\eta$, if the bin size is smaller than the typical range over which the parent rapidity distribution changes considerably. Dynamical fluctuations saturate the moments if $\delta\eta$ is smaller than this range. Hence for sufficiently small $\delta\eta$ values, the contribution of resonance decays which give rise to correlations on large scales can be neglected.

Evidence of intermittent behavior is obtained from the increase of fluctuations with decrease in bin size. It was shown [2] that intermittency leads to a power-law dependence on $\delta\eta$:

$$\langle F_q \rangle = (\Delta\eta/\delta\eta)^{\varphi_q} , \tag{2}$$

where φ_q is a measure of the strength of intermittency. The data were fitted to the relation

$$\ln\langle F_q \rangle = A - \varphi_q \ln\delta\eta , \tag{3}$$

where A is a constant. The relation (3) predicts a linear rise of $\ln\langle F_q \rangle$ with $-\ln\delta\eta$ for all bin widths down to the smallest value allowed by the experimental resolution or the statistical limit. The value of $\Delta\eta$ in our data ranges from 0.5 to 6.0. Figures 2(a) and 2(b) show the rising trend of $\ln\langle F_q \rangle$ with $-\ln\delta\eta$ for nucleon and AgBr targets. The increase is more in the case of nucleon targets. This can be seen quantitatively from Table II, which shows the slopes φ_q for qth order moments for nucleon and AgBr targets. The higher value of φ_q for nucleon targets show that the intermittency effect is more for hadron-hadron than for hadron-nucleus interactions. It has been found [5(b),24] that the intermittency signal is highest for elementary e^+e^- annihilations, followed by a

TABLE I. The event type, primary energy, and pseudorapidity values of the secondary particles for interactions with AgBr and with primary energy > 1 TeV.

Serial number	Event type	Primary energy (TeV)	Pseudorapidity values
1	16+14*p*	23.78	2.95,3.68,4.23,4.63,4.72,4.76,4.90,5.36,5.41,5.50,6.40,6.77,6.79, 6.79
2	9+24*p*	239.96	3.77,3.82,4.35,4.40,4.69,4.81,5.04,5.06,5.16,5.25,5.50,5.52,6.70, 7.11,7.14,7.34,7.37,7.41,8.29,8.49,8.75,9.21,9.44,9.48
3	11+15*n*	1.49	2.38,2.81,2.92,3.22,3.45,3.77,3.96,4.00,4.33,4.79,4.81,4.90,5.04, 5.13,5.22
4	12+20*p*	1.97	0.27,0.65,1.05,2.40,2.92,3.38,3.52,3.94,4.03,4.35,4.58,4.67, 4.83,4.83,4.95,5.09,7.32,7.32,7.37,7.39
5	12+12*p*	2.92	0.00,2.42,2.51,3.64,3.87,4.65,4.81,4.88,4.92,5.16,5.22,5.59
6	19+36*p*	3.84	1.58,2.04,2.11,2.20,2.36,2.40,2.65,2.76,2.81,2.88,2.88,2.99,3.13, 3.29,4.00,4.19,4.33,4.40,4.88,5.06,5.22,5.48,5.68,5.78,5.92,6.08, 6.12,6.21,6.26,6.40,6.44,6.47,6.63,6.67,6.77,7.55
7	14+15*p*	1.20	1.28,2.24,2.86,2.95,2.99,3.20,4.14,4.53,4.83,4.95,5.06, 5.11,5.11,5.29,5.45
8	12+12*p*	4.23	1.97,2.09,3.15,3.84,3.91,4.12,4.17,4.40,5.89,6.24,6.38,6.72
9	25+19*p*	2.71	1.42,1.63,1.75,2.04,2.88,2.95,4.12,4.30,4.35,5.04,5.22,5.27,5.36, 5.43,5.66,5.71,5.80,5.94,6.72
10	14+18*p*	1.94	1.36,2.22,2.51,2.70,2.79,2.90,3.13,3.57,3.87,4.42,4.88,4.99,5.06, 5.52,5.55,5.57,5.80,6.24
11	17+31*p*	3.17	1.12,1.44,2.17,2.58,2.67,2.99,3.04,3.75,3.82,3.91,4.12,4.14, 4.35,4.49,4.58,4.60,4.97,5.04,5.06,5.11,5.25,5.27,5.34,5.43,5.57,5.87,6.03, 6.19,6.86,7.43
12	16+45*p*	98.67	0.48,1.63,2.70,2.95,3.45,3.91,4.12,4.21,4.37,4.42,4.56,4.76,4.83, 5.34,5.43,5.52,5.66,5.73,5.75,5.94,6.01,6.42,6.49,6.51,6.63,6.67, 6.72,6.79,6.93,7.04,7.11,7.16,7.32,7.34,7.53,7.64,7.83,8.03,8.06,8.52, 8.54,8.66,8.75,8.98,9.02
13	19+13*p*	1.49	2.20,2.26,2.88,3.36,3.75,4.00,4.12,4.63,5.04,5.06,5.29,5.41,5.94
14	16+54*n*	2.88	0.45,0.91,1.10,1.54,1.65,1.75,1.84,2.17,2.31,2.40,2.51,2.65, 2.74,2.76,2.81,3.06,3.22,3.29,3.43,3.45,3.59,3.66,3.68,3.75,3.87,3.91, 3.96,4.14,4.35,4.42,4.56,4.60,4.83,5.09,5.41,5.68,5.73.,5.78,6.01, 6.21,6.33,6.33,6.38,6.42,6.49,6.56,6.63,6.67,6.97,7.25,7.64,7.80, 7.87,7.99
15	19+31*p*	3.83	0.96,1.89,2.56,2.67,2.81,2.90,3.25,3.27,3.31,3.41,3.71,3.98, 4.03,4.14,4.17,4.19,4.28,4.37,4.74,5.25,5.27,5.29,5.64,5.98,6.03,6.03, 6.19,6.95,7.14,7.23,7.37
16	10+15*p*	1.06	0.00,0.80,0.96,2.29,2.38,3.38,4.00,4.37,4.56,4.81,4.95,4.99,5.18, 5.64,5.71
17	16+25*n*	1.00	0.00,0.77,1.40,1.44,2.02,2.54,3.22,3.41,3.52,3.64,3.66,3.68, 3.98,4.07,4.53,4.65,4.76,4.83,4.88,4.90,4.95,4.97,5.04,5.13,5.57
18	11+11*p*	4.49	1.44,1.63,3.80,4.51,4.56,5.32,5.43,5.57,5.64,5.68,5.80
19	15+29*p*	15.42	0.00,1.38,2.79,3.27,3.73,4.12,4.21,4.37,4.49,4.56,4.74,4.81,5.04, 5.13,5.41,5.41,5.52,5.52,5.78,5.78,6.01,6.38,6.40,6.47,6.49, 6.61,6.67,6.67,6.91
20	11+21*p*	3.15	0.00,2.79,2.95,3.20,3.22,3.36,3.43,3.45,3.59,3.66,3.68,3.82,4.40, 4.76,5.09,5.27,5.50,5.71,6.19,6.47,6.88
21	13+36*n*	1.85	1.44,1.50,1.60,2.26,2.36,2.47,2.56,2.67,2.97,2.99,3.27,3.31, 3.45,3.48,3.66,3.68,3.91,3.96,4.23,4.28,4.65,4.90,4.95,4.97,5.06,5.06, 5.18,5.27,5.71,5.71,5.96,6.08,6.12,6.42,6.44,6.47
22	15+47*p*	12.23	0.00,0.98,1.60,2.31,2.45,2.56,2.74,2.79,2.88,3.68,3.82,3.87,3.91, 4.30,4.33,4.33,4.35,4.53,4.63,4.83,5.02,5.02,5.04,5.06,5.25,5.29,5.66, 5.66,5.71,5.75,5.78,5.92,6.03,6.03,6.08,6.24,6.38,6.42,6.47,6.84, 7.04,7.11,7.20,7.39,7.60,7.64,7.92
23	10+11*p*	9.44	1.65,1.78,2.95,3.50,4.72,4.76,5.32,5.41,6.58,6.84,7.37
24	9+21*p*	3.28	1.69,2.31,3.11,3.73,3.87,3.89,3.89,3.91,3.96,4.07,4.17,4.46, 4.56,5.20,5.25,5.29,5.41,5.43,5.71,5.94,6.10
25	10+16*n*	3.20	1.42,2.88,3.41,3.80,3.84,4.07,4.28,4.51,4.72,4.90,5.18,5.25,5.48, 5.92,6.10,6.15
26	14+17*n*,*p*	5.33	2.47,3.48,3.94,4.26,4.33,4.37,4.44,4.74,4.79,4.88,4.99,5.04,5.09, 5.18,5.25,5.39,5.45

TABLE I. (*Continued*).

Serial number	Event type	Primary energy (TeV)	Pseudorapidity values
27	$23+15p$	13.47	3.66,3.68,3.82,4.14,4.40,4.65,4.88,5.04,5.25,5.29,6.47, 6.51,6.72,6.84,8.72
28	$10+18p$	1.13	1.22,1.60,1.65,2.11,2.70,2.79,2.81,3.64,4.33,4.56,4.79,5.09, 5.22,5.27,5.41,5.62,6.91
29	$16+68p$	2.55	0.78,1.14,1.14,1.16,1.33,1.36,1.97,1.97,2.20,2.22,2.42,2.45, 2.65,2.65,2.65,2.65,2.65,2.88,2.88,3.11,3.11,3.36.3.57,3.57,3.57,3.57,3.59, 3.80,3.80,3.80,4.03,4.26,4.26,4.26,4.26,4.49,4.49,4.49,4.72,4.72,4.72 4.83,4.95,4.95,4.95,5.18,5.20,5.41,5.64,5.64,5.64,5.64,5.87,5.87,5.89, 6.33,6.79,6.79,6.79,7.02,7.02,7.25,7.25,7.25,7.71,7.71.8.24
30	$20+192n$	1.61	0.00,0.67,0.68,0.71,0.72,0.77,0.81,1.01,1.05,1.10,1.14,1.20,1.26, 1.29,1.40,1.42,1.52,1.56,1.65,1.67,1.73,1.78,1.82,1.84,1.91,1.93,1.97, 2.06,2.09,2.09,2.13,2.33.2.38,2.40,2.47,2.49,2.54,2.58,2.58,2.63,2.63, 2.65,2.67,2.72,2.72,2.74,2.74,2.76,2.76,2.79,2.79,2.81,2.83,2.88, 2.95,2.95,2.97,2.99,3.02,3.04,3.06,3.08,3.08,3.13,3.22,3.27,3.27,3.34,3.41, 3.43,3.48,3.50,3.52,3.52,3.54,3.57,3.61,3.64,3.66,3.68,3.68, 3.73,3.77,3.80,3.84,3.87,3.89,3.91,3.94,3.94,3.94,3.94,3.96,3.98, 3.98,4.00,4.00,4.03,4.05,4.05,4.07,4.07,4.07,4.07,4.10,4.12,4.12,4.14, 4.17,4.19,4.26,4.28,4.28,4.33,4.37,4.40,4.42,4.44,4.49,4.51, 4.58,4.60,4.67,4.72,4.72,4.79,4.79,4.79,4.83,4.86,4.88,4.95,5.02, 5.02,5.04,5.04,5.04,5.06,5.18,5.18,5.27,5.27,5.29,5.32,5.34,5.36, 5.41,5.50,5.59,5.68,5.71,5.71,5.73,5.75,5.75,5.78,5.78,5.80,5.85, 5.89,5.96,5.98,6.01,6.05,6.17,6.21,6.40,6.47,6.49,6.49,6.61,6.65, 6.67,6.70,6.72,6.86,6.88,7.09,7.14,7.32,7.34,7.37,7.57,7.60,7.73, 7.78,7.87,8.17,8.24

lower signal for hadron-hadron collisions and a further decrease of the signal for nucleus-nucleus interactions. This probably shows that intermittency is taking place at the parton level. As the complexity of the projectile and target increases, the intermittency signal could get diluted due to multinucleon collisions.

Figures 3(a) and 3(b) show the respective variation of $\ln\langle F_q\rangle$ as a function of $-\ln\delta\eta$ for events with primary energies $E_p<1$ TeV and $E_p>1$ TeV for AgBr targets. The error bars in both the figures represent the standard errors. The reason for choosing AgBr as the target for primary energy dependence is that the interactions with AgBr ($N_h\geq 9$) can be unambiguously identified in nuclear emulsion. Keeping the target same, any difference in the distributions will directly reflect the difference due to different primary energies. Although the errors in Fig. 3(b) are large due to low statistics, the increasing trend of $\ln\langle F_q\rangle$ with $-\ln\delta\eta$ is clear from Figs. 3(a) and 3(b). Table II also shows the values of the slopes φ_q for $q=2$–5, at primary energies of $E_p<1$ TeV and $E_p>1$ TeV. With the increase in primary energy, the slopes show a decreasing trend for each value of q. A similar primary energy dependence of the slopes has been reported by the UA1 Collaboration [5(a)].

The scaling behavior of factorial moments has been related to the physics of fractal objects (particle emission sources), through the anomalous dimension d_q which has been computed from the slopes φ_q by the relation [25]

$$d_q=\frac{\varphi_q}{q-1}\ . \tag{4}$$

Figure 4 shows the values of d_q versus q ($q=2$–5) for nucleon and AgBr targets, the errors being standard. The rising pattern of d_q with q reflects the self-similar cascade mechanism. These observations are in agreement with the results from lepton-hadron and hadron-hadron interactions [26]. With the increase in target mass, the dimension d_q decreases for each order of the moments. Figure 5 shows a similar behavior of d_q with q for interactions with $E_p<1$ TeV and $E_p>1$ TeV for AgBr targets. The dimension d_q is found to decrease with increase in primary energy.

Bialas and Zalewski [18] have studied the phase structure of self-similar multiparticle systems using the random cascading model [1,27]. The importance of this model lies in its ability to reproduce the fundamental property of intermittent behavior, i.e., the power-law dependence of the scaled moments of particle density on the bin size. It was suggested [18] that the function

$$\lambda_q=\frac{\varphi_q+1}{q} \tag{5}$$

should reflect the structure of the system in the regions $q<q_c$ and $q>q_c$, where q_c is some minimum point in the distribution. The regions $q<q_c$ and $q>q_c$ are, respectively, dominated by numerous fluctuations and small number of sometimes large fluctuations. The system resembles a mixture of a "liquid" of many small fluctuations and a "dust" of high density. We see either liquid or dust phase, depending upon whether we probe the system by a moment of rank $q<q_c$ or $q>q_c$. Thus the

probe, i.e., the selected moment of the density is sensitive to either one of the two phases. Peschanski [28] has suggested that the observation of a minimum in the λ_q versus q distribution would suggest a phase transition.

Figure 6(a) shows a plot of λ_q versus q for nucleon and AgBr targets. The solid line represents the nonexistence of intermittency. It is seen that λ_q values for both the targets lie away from this solid line. Thus this distribution also brings out the intermittent behavior of the two classes of interactions. It is found that the value of φ_q(nucleon targets) $>\varphi_q$(AgBr targets) for each order of the moment. No minimum value of λ_q for a certain value of $q=q_c$ is observed for interactions with nucleon and AgBr targets. This indicates the absence of nonthermal phase transition. Our results are in agreement with the data from the NA22, KLM, and European Muon Collaborations (EMC) [18]. Figure 6(b) shows the behavior of λ_q versus q for interactions with $E_p<1$ TeV and $E_p>1$ TeV. In both cases, a departure from no intermittency line is seen, the effect being stronger for $E_p<1$ TeV as compared to $E_p>1$ TeV events. In both Figs. 6(a) and 6(b), the errors are too small to be plotted.

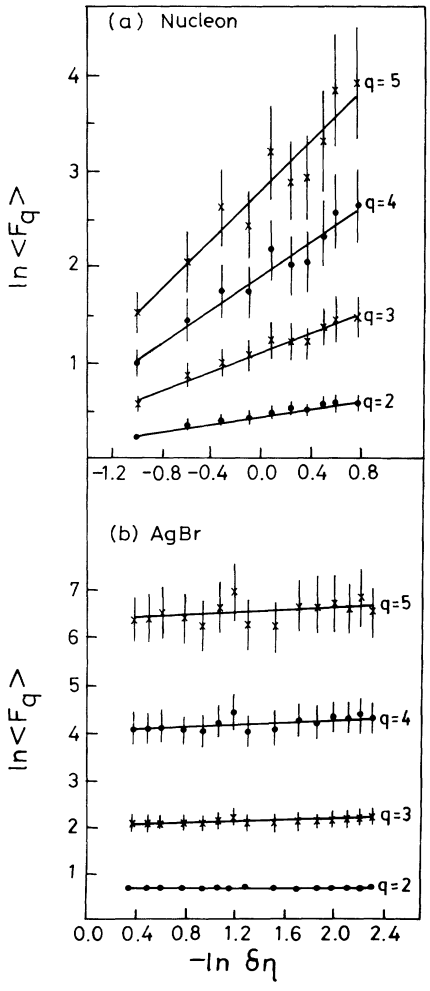

FIG. 2. $\ln\langle F_q\rangle$ as a function of $-\ln\delta\eta$ for (a) nucleon interactions and (b) AgBr interactions. The solid lines indicate the least-square fits to the data points.

IV. COMPARISON WITH THE JACEE EVENT

In order to see the rapidity fluctuations in individual events, we show in Fig. 1 the pseudorapidity distributions for a few representative events. The value of the multiplicity and the primary energy for each event are given in the figure. Sharp spikes in the η distribution are clearly evident, which are washed out when we plot η for all the events. Rapidity fluctuations in any given event (horizontal fluctuations) can be studied from the rapidity distributions for each event separately.

The 5 TeV/nucleon Si+AgBr cosmic ray event observed by the JACEE Collaboration [1] is unique in that it has a shower particle multiplicity >1000 and it also provided the first experimental evidence of rapidity fluctuations. This event hereafter will be called the JACEE event. The cosmic ray interactions at $E_p>1$ TeV investigated here are in the same energy range as the JACEE event and hence a comparison of the two would be interesting. Comparing the rapidity distributions of the JACEE event with some of the present events with $E_p>1$ TeV (Fig. 1), we find that despite the exceptionally large difference in multiplicities of the two types of events, they show similar rapidity fluctuations. This similarity together with the original analysis of the JACEE event by Bialas and Peschanski [2] reinforces the dynamical origin of rapidity fluctuations. Further, we find that the pseudorapidity distributions are relatively more inhomogeneous in the present events as compared to the JACEE event, which can be attributed to the smaller multiplicity of the former events as compared to the latter event. This effect is also clear from the values of the slopes φ_q, which signify the degree of intermittency. In particular, φ_5 for $E_p>1\text{TeV}=0.539$ and from the Bialas and Peschanski [2] analysis of the JACEE event, $\varphi_5\sim 0.144$.

V. MULTIFRACTALITY

The prescription provided by Chiu and Hwa [10] for investigating the multifractality relies on the G_q moments which can be directly determined from experiments. The advantage of these moments is that the power-law behavior of G_q is to be analyzed event by event, whereas the event averaged distribution suppresses fluctuations in individual events.

Let $\Delta\eta$ be the pseudorapidity interval in which we wish to carry out the multifractal analysis. Let $\Delta\eta$ be subdivided into M bins each of width $\delta\eta=\Delta\eta/M$. Let N be the number of particles in one event in the pseudorapidity range $\Delta\eta$ and k_m be the number of particles in the mth bin. The multifractal moment G_q is defined as [10]

$$G_q=\sum_{m=1}^{m}\left[\frac{k_m}{N}\right]^q=\sum_{m=1}^{m}p_m^q\ , \tag{6}$$

where $p_m=k_m/N$ is the probability of particles in the mth bin for one event and q is any real number, positive or negative. The summation in Eq. (6) is carried over nonempty bins only, which we assume are m in number and constitute a set of bins that have fractal properties in the large M limit. If the particle production process ex-

TABLE II. Values of the slopes φ_q obtained from least-squares fits of Eq. (3) (text) to the data for the qth-order scaled factorial moments [Eq. (1) in the text] for different targets and primary energies. The errors are standard.

Category	φ_2	φ_3	φ_4	φ_5
Nucleon	0.194±0.015	0.487±0.032	0.864±0.075	1.268±0.147
AgBr	0.018±0.006	0.076±0.019	0.142±0.045	0.170±0.089
$E_p<1$ TeV, AgBr	0.174±0.025	0.412±0.064	0.697±0.112	0.985±0.169
$E_p>1$ TeV, AgBr	0.032±0.019	0.133±0.074	0.309±0.169	0.539±0.303

hibits self-similar behavior, then the moment follows the relation [10],

$$G_q \propto (\delta\eta)^{\tau(q)} . \tag{7}$$

The power-law behavior in Eq. (7) is not achieved if $\delta\eta \to 0$. Hence we consider the region where M is not very large. We determine $\langle \ln G_q \rangle$ for an ensemble of events, using

$$\langle \ln G_q \rangle = \frac{1}{N_{\rm ev}} \sum_{N_{\rm ev}} \ln G_q , \tag{8}$$

where the summation is carried out over the events $N_{\rm ev}$. By plotting $\langle \ln G_q \rangle$ versus $-\ln\delta\eta$, we obtain the average slope $\langle \tau(q) \rangle$, given by Eq. (7).

Using Eq. (8) the value of $\langle \ln G_q \rangle$ is calculated for events with q ranging from -6.0 to 6.0. The step size is 0.5 except in the region $-1.0 < q < 1.0$, where the step size is 0.1. Figures 7(a) and 7(b) show the values of $\langle \ln G_q \rangle$ as a function of $-\ln\delta\eta$ for interactions with nucleon and AgBr targets, respectively. The values of $\langle \ln G_q \rangle$ are plotted only for a few values of q in the interest of clarity. For the same reason, only some representative errors are plotted in the two figures. The statistical errors are lowest for AgBr targets (8%) and increase for nucleon (15%) targets. The higher number of events for AgBr targets lead to a consequent lowering of the statistical errors. The distributions in Fig. 7 show a saturation behavior in the large $-\ln\delta\eta$ region for low values of $q(q<1)$. Early saturation for nucleon targets [Fig. 7(a)] compared to AgBr targets [Fig. 7(b)] can be explained due to more low multiplicity events in the former than in the latter class of interactions. In order to investigate the primary energy dependence of the multifractal

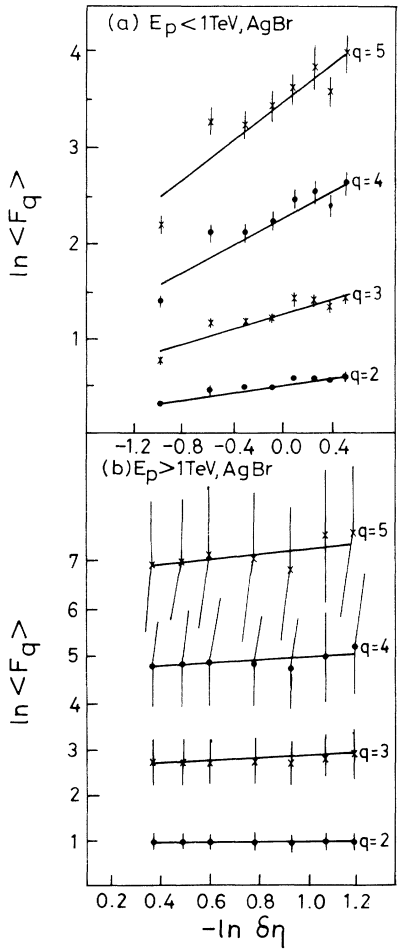

FIG. 3. $\ln\langle F_q \rangle$ as a function of $-\ln\delta\eta$ for (a) $E_p<1$ TeV, AgBr interactions and (b) $E_p>1$ TeV, AgBr interactions. The solid lines indicate the least-square fits to the data points.

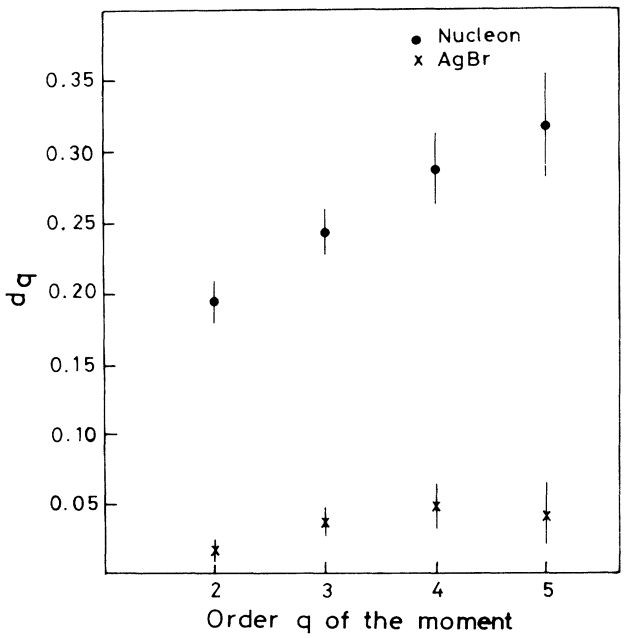

FIG. 4. The anomalous fractal dimension d_q as a function of q (order of the moments) for nucleon interactions (circles) and AgBr interactions (crosses) for the scaled factorial moments.

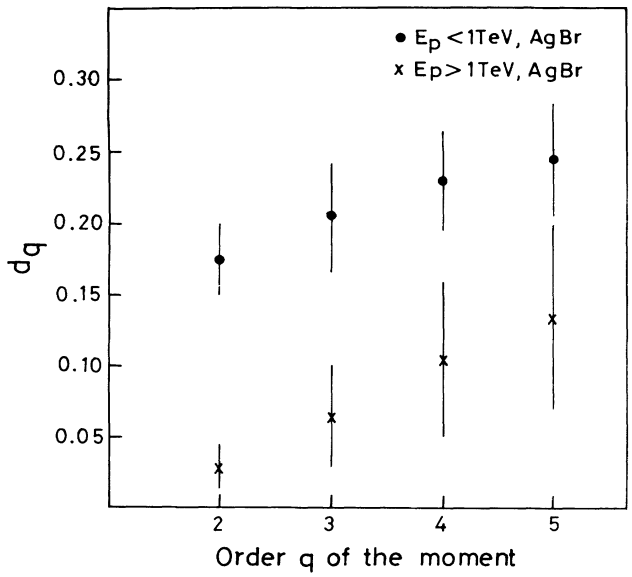

FIG. 5. The anomalous fractal dimension d_q as a function of q (order of the moments) for $E_p < 1$ TeV, AgBr interactions (circles) and $E_p > 1$ TeV, AgBr interactions (crosses) for the scaled factorial moments.

structure in the events, we determine the multifractal moments $\langle \ln G_q \rangle$ for events with $E_p < 1$ TeV and $E_p > 1$ TeV, for $q = -6.0$–6.0. Figure 8 shows the values of $\langle \ln G_q \rangle$ versus $-\ln\delta\eta$ for interactions with AgBr nuclei with the above primary energies. It is clear from Fig. 8 that for large values of $-\ln\delta\eta$ and $q < 1$, the distributions saturate. Early saturation for $E_p < 1$ TeV events as compared to $E_p > 1$ TeV events is due to the presence of more low multiplicity events in the former as compared to the latter events. The statistical errors are 10% for $E_p < 1$ TeV and 19% for $E_p > 1$ TeV events.

As discussed earlier, the average slopes $\langle \tau(q) \rangle$ are calculated by the method of least-square fit to the data for $M = 1$–8. The generalized dimension (Renyi dimension) is related to the slope $\langle \tau(q) \rangle$ by [29]

$$D_q = \frac{\langle \tau(q) \rangle}{q-1} . \tag{9}$$

Using Eq. (9), the generalized dimension D_q is calculated for nucleon and AgBr targets and plotted in Fig. 9 as a function of q, the order of the moments. As the target mass increases, $\langle N_s \rangle$ increases and hence the dimension D_q also increases. Our results on D_q are in agreement with the data from 800 GeV proton-nucleus interactions [6(c)]. Figure 10 shows D_q versus q for interactions with

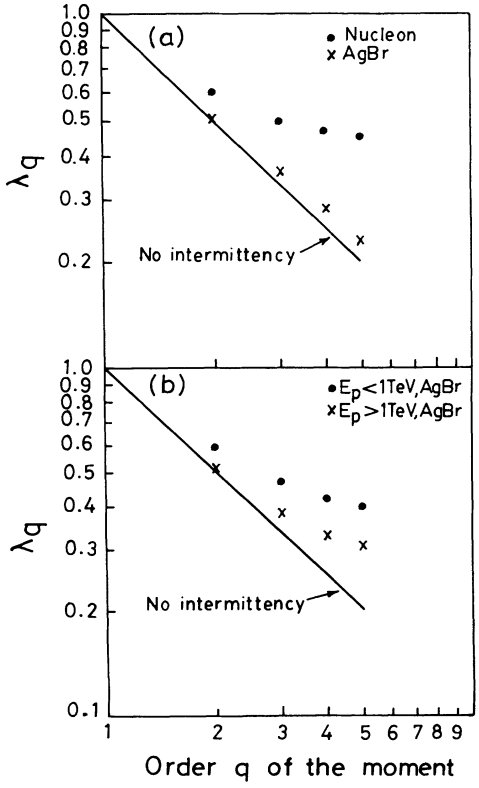

FIG. 6. λ_q as a function of q (order of the moments) for (a) nucleon interactions (circles) and AgBr interactions (crosses) and (b) $E_p < 1$ TeV, AgBr interactions (circles) and $E_p > 1$ TeV, AgBr interactions (crosses).

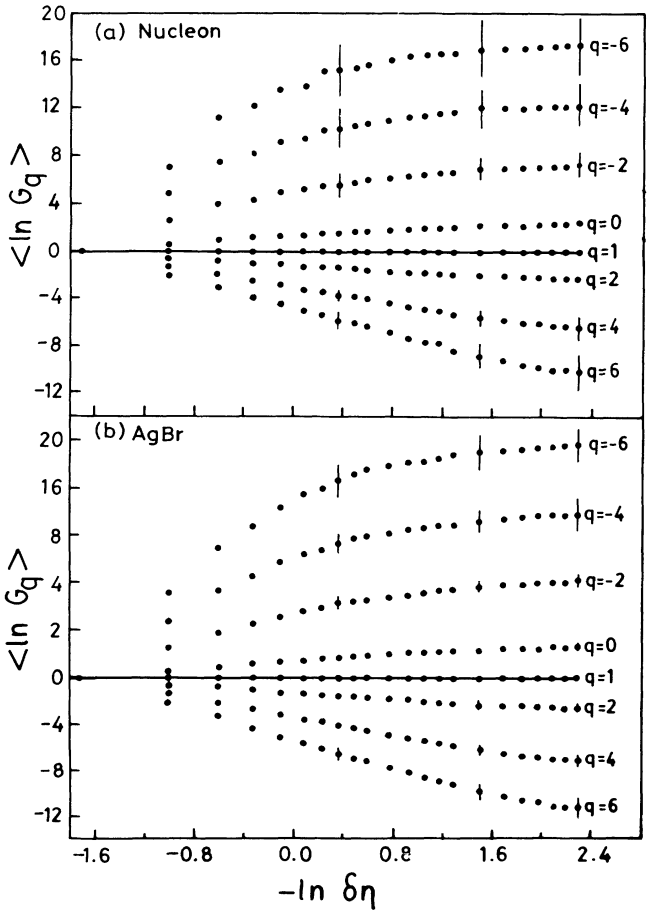

FIG. 7. $\langle \ln G_q \rangle$ as a function of $-\ln\delta\eta$ for (a) nucleon interactions and (b) AgBr interactions.

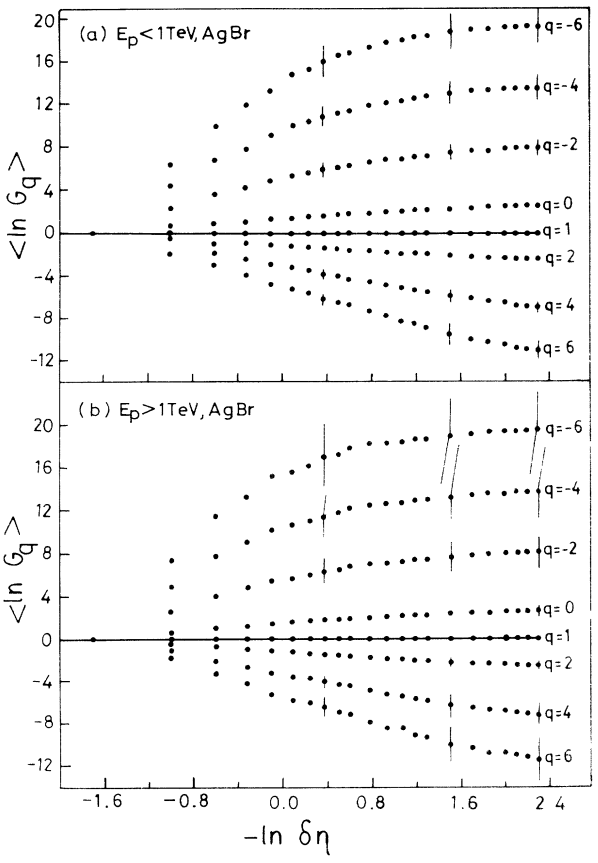

FIG. 8. $\langle \ln G_q \rangle$ as a function of $-\ln\delta\eta$ for (a) $E_p < 1$ TeV AgBr interactions and (b) $E_p > 1$ TeV, AgBr interactions.

AgBr targets for $E_p < 1$ TeV and $E_p > 1$ TeV. With increase in primary energy, $\langle N_s \rangle$ increases and hence the dimension D_q also increases.

The number m of nonempty bins constitute a set of bins that have fractal properties, when M becomes large. Let each bin be described by a power-law behavior [10]

$$p_m \propto (\delta\eta)^{\alpha_q} . \tag{10}$$

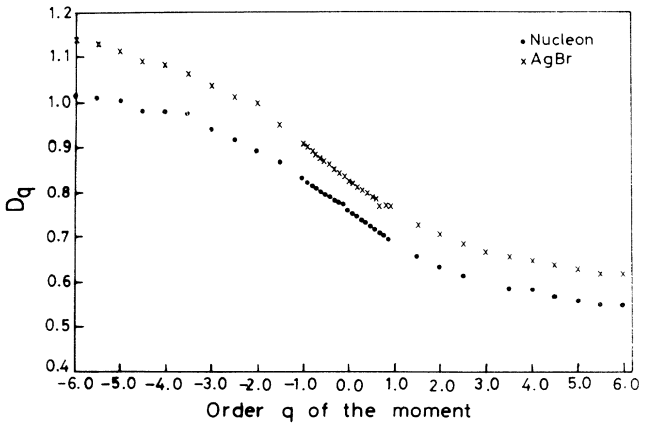

FIG. 9. The generalized dimensions (Renyi dimensions) D_q as a function of q (order of the moments) for nucleon interactions (circles) and AgBr interactions (crosses).

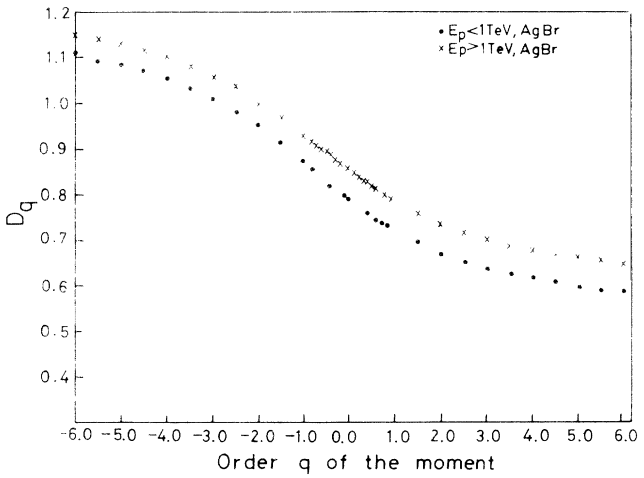

FIG. 10. The generalized dimensions (Renyi dimensions) D_q as a function of q (order of the moments) for $E_p < 1$ TeV, AgBr interactions (circles) and $E_p > 1$ TeV, AgBr interactions (crosses).

Several bins having the same behavior as Eq. (10) can each be mapped into interval $[\alpha_q, \alpha_q + d\alpha_q]$. The collection of all such bins constitutes a fractal subset, which is labeled by the index α_q. Let the number of bins of such a subset be M_α, whose dependence on $\delta\eta$ is given by [10]

$$M_{\alpha_q} \propto \delta\eta^{-f(\alpha_q)} . \tag{11}$$

All subsets M_α of M constitute the multifractal structure of the rapidity distribution. In order to determine the spectrum $f(\alpha_q)$ of all α_q indices, we calculate $f(\alpha_q)$ by the relations [10]

$$f(\alpha_q) = q\alpha_q - \tau(q) \tag{12}$$

and

$$\alpha_q = \frac{d\tau(q)}{dq} . \tag{13}$$

The value of $\tau(q)$ is determined for small incremental changes in q near the region $q=0$, where $f(\alpha_q)$ has its maximum. Using the relations (12) and (13), the values of α_q and $f(\alpha_q)$ are determined for nucleon and AgBr targets. Figure 11(a) shows the spectrum $f(\alpha_q)$ as a function of α_q for the two cases.

As expected [10] from the theory of multifractal structure, the spectrum $f(\alpha_q)$ shown in Fig. 11(a) is concave for the two cases. The distribution is centered at $\alpha_{q=0}$, which is in agreement with the gluon model [10]. The 45° line is tangent to the peaks of the spectrum $f(\alpha_q)$ at $\alpha_{q=1}$ for nucleon and AgBr targets. This is a general property of the multifractals [10]. In the $f(\alpha_q)$ spectrum, the left wing ($q > 0$) describes the peaks and the right wing ($q < 0$) describes the valleys of the single-particle pseudorapidity distribution of the particular events. The width of the spectrum $f(\alpha_q)$ reflects the inhomogeneity [13] of the pseudorapidity distribution.

The $f(\alpha_q)$ spectrum is broader for nucleon targets than for AgBr targets. Thus, the single-particle η distri-

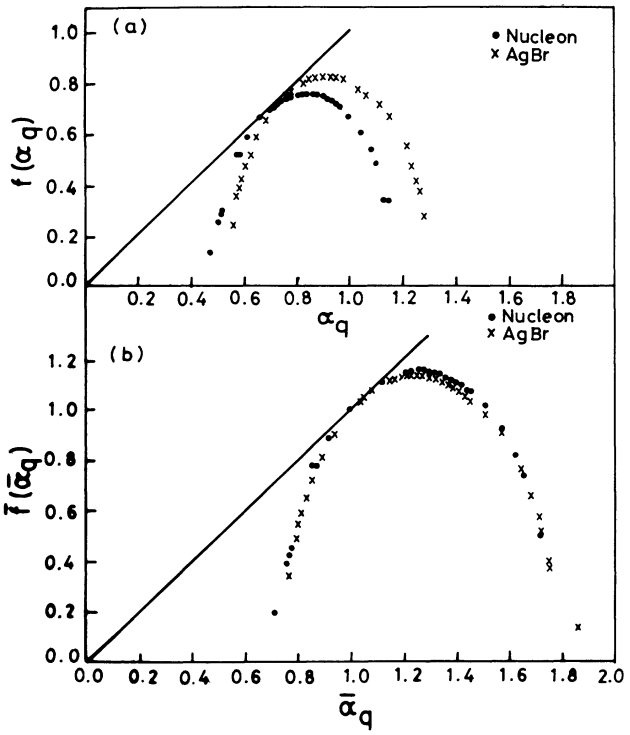

FIG. 11. (a) The spectrum $f(\alpha_q)$ as a function of α_q and (b) the rescaled spectrum $\bar{f}(\bar{\alpha}_q)$ as a function of $\bar{\alpha}_q$ for nucleon interactions (circles) and AgBr interactions (crosses).

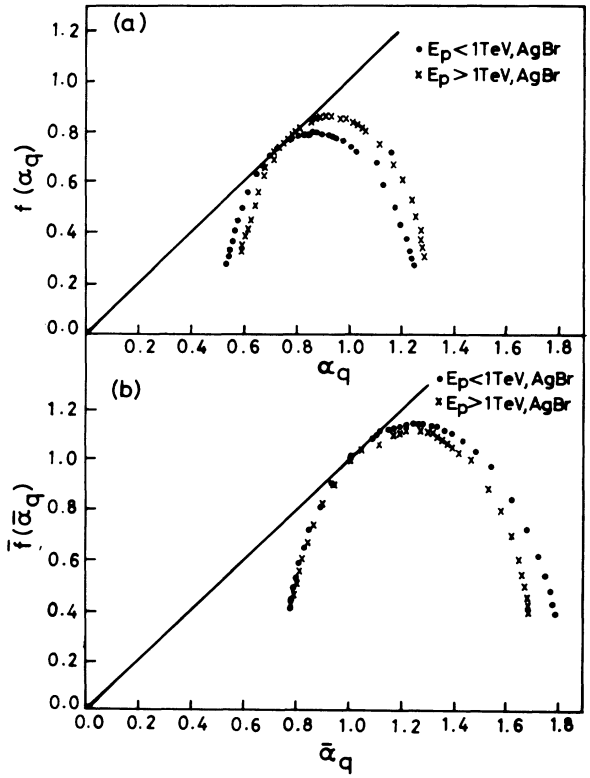

FIG. 12. (a) The spectrum $f(\alpha_q)$ as a function of α_q and (b) and rescaled spectrum $\bar{f}(\bar{\alpha}_q)$ as a function of $\bar{\alpha}_q$ for $E_p < 1$ TeV, AgBr interactions (circles) and $E_p > 1$ TeV, AgBr interactions (crosses).

bution for interactions with nucleon target is more inhomogeneous than that for interactions with the AgBr target. The chaotic nature of the η distribution can be well described by the smooth $f(\alpha_q)$ spectrum. From the spectrum $f(\alpha_q)$ we determined the fractal dimension, $D_0=f(\alpha_0)$, the information dimension, $D_1=f(\alpha_1)$ and the correlation dimension $D_2=2\alpha_2-f(\alpha_2)$. These three dimensions are sensitive to the process of multiparticle production. The values of D_0, D_1, and D_2 for nucleon and AgBr targets are shown in Table III. It is clear that with increase in target mass and primary energy, the values of these dimensions tend to increase.

In order to understand the relationship between the spectra for different targets, we rescale the spectrum $f(\alpha_q)$ in Fig. 11(a) using the relations [19]

$$\bar{\alpha}_q=\alpha_q/\alpha_1 \tag{14}$$

and

$$\bar{f}(\bar{\alpha}_q)=\frac{f(\alpha_q)}{f(\alpha_1)}=\frac{f(\alpha_q)}{\alpha_1} . \tag{15}$$

The rescaled spectrum $\bar{f}(\bar{\alpha}_q)$ for interactions with nucleon and AgBr targets is shown in Fig. 11(b). The two curves coincide for $\bar{\alpha}_q<1$ ($q>1$). This shows universality of the multifractal structure in this region for both nucleon and AgBr targets. Since the region $q>1$ describes the peaks of the pseudorapidity distribution, we find the universality in this region for both types of targets. For $\bar{\alpha}_q>1$ ($q<1$) there is less space in the $q<1$ region for interactions with AgBr as compared to nucleon targets. The $f(\alpha_q)$ spectrum and its rescaled spectrum for $E_p<1$ TeV and $E_p>1$ TeV are shown in Figs. 12(a) and 12(b), respectively. The broadening of the $f(\alpha_q)$ spectrum with

TABLE III. Values of various dimensions (D_q) obtained from the spectrum $f(\alpha_q)$ [Eq. (12) in the text] for different targets and primary energies. The errors are statistical.

Category	Fractal dimension $D_0=f(\alpha_0)$	Information dimension $D_1=f(\alpha_1)$	Correlation dimension $D_2=2\alpha_2-f(\alpha_2)$
Nucleon	0.764±0.117	0.661±0.102	0.637±0.098
AgBr	0.832±0.071	0.732±0.062	0.708±0.060
$E_p<1$TeV, AgBr	0.796±0.078	0.698±0.069	0.675±0.066
$E_p>1$TeV, AgBr	0.859±0.165	0.763±0.146	0.740±0.142

an increase in the primary energy is clear from Fig. 12. From Fig. 12(b) it is found that for $\bar{\alpha}_q < 1$ ($q > 1$) both the curves coincide which indicates universality of the multifractal structure. In the region $\bar{\alpha}_q > 1$ ($q < 1$), the rescaled spectrum $\bar{f}(\bar{\alpha}_q)$ has a greater space for $E_p < 1$ TeV as compared to events with $E_p > 1$ TeV. Hence there are more valleys in the pseudorapidity distribution of events with $E_p < 1$ TeV as compared to those with $E_p > 1$ TeV. The $\bar{f}(\bar{\alpha}_q)$ spectra are wide enough to resemble a multifractal multiplicity fluctuation.

VI. CONCLUSIONS

Intermittency and multifractality for interactions with nucleon and AgBr targets at different primary energies (< 1 TeV and > 1 TeV) have been studied. An intermittent pattern is observed for both nucleon as compared to AgBr interactions. The slopes φ_q decrease with increase in primary energy. From the behavior of anomalous dimension d_q, the particle production is attributed to the self-similar cascade mechanism. The dimension d_q is found to decrease with increase in primary energy. The pattern of λ_q versus q shows a clear signal of intermittency and there is no evidence of phase transition for events with different targets and different primary energies.

The observation of the power-law behavior of the G_q moments suggest a multifractal behavior. The generalized dimension (Renyi dimension) D_q increases as the target mass increases. The observed behavior of D_q is in agreement with the multifractal cascade model. D_q also increases with increase in primary energy.

The function $f(\alpha_q)$ completely describes the dynamics of the particle production processes. Depending upon the probe, i.e., the value of q, we can map out the whole of the pseudorapidity distribution from the spectrum $f(\alpha_q)$. The width of the spectrum $f(\alpha_q)$ is more for nucleon than for AgBr targets, signifying that the η distribution is more inhomogeneous for the former as compared to the latter events. The rescaled spectrum $\bar{f}(\bar{\alpha}_q)$ shows universality of the multifractal structure for $\bar{\alpha}_q < 1$ ($q > 1$) for nucleon and AgBr targets and for $E_p < 1$ TeV and $E_p > 1$ TeV interactions. The $\bar{f}(\bar{\alpha}_q)$ spectra are wide enough to signify that the multiplicity fluctuations are multifractal and not monofractal.

Finally, multifractality in the theory of chaos has the potential to help in unraveling the underlying mechanism for multiplicity fluctuations.

[1] JACEE Collaboration, T. H. Burnett *et al.*, Phys. Rev. Lett. **50**, 2062 (1983).

[2] A. Bialas and R. Peschanski, Nucl. Phys. **B273**, 703 (1986); **B308**, 857 (1988).

[3] B. L. Hao, *Chaos* (World Scientific, Singapore, 1984).

[4] (a) B. Buschbeck, P. Lipa, and R. Peschanski, Phys. Lett. B **215**, 788 (1988); (b) D. De Camp *et al.*, Z. Phys. C **53**, 21 (1992).

[5] (a) UA1 Collaboration, C. Albajar *et al.*, Nucl. Phys. **B345**, 1 (1990); (b) J. B. Singh and J. M. Kohli, Phys. Lett. B **261**, 160 (1991); (c) EHS/NA22 Collaboration, N. M. Agababyan *et al.*, *ibid.* **261**, 165 (1991).

[6] (a) KLM Collaboration, R. Holynski *et al.*, Phys. Rev. Lett. **62**, 733 (1989); Phys. Rev. C **40**, R2449 (1989); (b) EHS/NA22 Collaboration, F. Botterweck *et al.*, Z. Phys. C **51**, 37 (1991); (c) R. K. Shivpuri and V. K. Verma, Phys. Rev. D **47**, 123 (1993).

[7] WA80 Collaboration, R. Abrecht, Phys. Lett. B **221**, 427 (1989); EMU01 Collaboration, E. Stenlund *et al.*, in *Quark Matter '88,* Proceedings of the Seventh International Conference on Ultrarelativistic Nucleus-Nucleus Collisions, Lenox, Massachusetts, 1988, edited by G. Baym, P. Braun-Munzinger, and S. Nagamiya [Nucl. Phys. **A498**, 541c (1989)]; EMU01 Collaboration, M. I. Admovich *et al.*, Phys. Rev. Lett. **65**, 412 (1990); Phys. Lett. B **242**, 512 (1990); **263**, 539 (1991); Z. Phys. C **49**, 395 (1991).

[8] B. B. Mandelbrot, *The Fractal Geometry of Nature* (Freeman, New York, 1977).

[9] G. Paladin and A. Vulpiani, Phys. Rep. **156**, 147 (1987).

[10] C. B. Chiu and R. C. Hwa, Phys. Rev. D **43**, 100 (1991).

[11] P. Carruthers and Minh Duong-Van, Los Alamos Report No. LA-UR-83-2419 (unpublished).

[12] P. Grassberger and I. Procaccia, Physica D **13**, 34 (1984); T. C. Halsey *et al.*, Phys. Rev. A **33**, 1141 (1986); Physica D **23**, 112 (1986).

[13] R. C. Hwa, Phys. Rev. D **41**, 1456 (1990).

[14] K. Sugano, in *Intermittency in High Energy Collisions,* Proceedings of the Marburg Workshop on Correlations and Multiparticle Production, Marburg, Germany, 1990, edited by M. Plumer, S. Raha, and R. Wiener (World Scientific, Singapore, 1991).

[15] UA1 Collaboration, H. Dibon and M. Markytan, in *Intermittency in High Energy Collisions,* Proceedings of the Santa Fe Workshop, Santa Fe, New Mexico, 1990, edited by F. Cooper, R. C. Hwa, and I. Sarcevic (World Scientific, Singapore, 1991); CDF Collaboration, F. Rimondi, in *Intermittency in High Energy Collisions* [14].

[16] W. Kittel, in *Quark Gluon Plasma,* edited by R. C. Hwa (World Scientific, Singapore, 1990).

[17] I. Derado, R. C. Hwa, G. Jancso, and N. Schmitz, Phys. Lett. B **283**, 151 (1992); I. Derado, J. Figiel, G. Jancso, and N. Schmitz, Z. Phys. C **54**, 357 (1992); N. Schmitz, in *Fluctuations and Fractal Structure,* Proceedings of the Ringberg Workshop on Multiparticle Production, Ringberg Castle, Germany, 1991, edited by R. C. Hwa, W. Ochs, and N. Schmitz (World Scientific, Singapore, 1992).

[18] A. Bialas and K. Zalewski, Phys. Lett. B **238**, 413 (1990).

[19] C. B. Chiu and R. C. Hwa, Phys. Rev. D **45**, 2276 (1992).

[20] ICEF Collaboration, F. Brisbout *et al.*, Nuovo Cimento Suppl. **1**, 1039 (1963).

[21] C. Gupt, R. K. Shivpuri, N. S. Verma, and A. P. Sharma, Phys. Rev. D **26**, 2202 (1982).

[22] C. Castagnoli *et al.*, Nuovo Cimento **10**, 1539 (1953).

[23] R. K. Shivpuri *et al.*, Phys. Rev. D **14**, 3103 (1976).

[24] TASSO Collaboration, W. Braunschweig *et al.*, Phys. Lett. B **231**, 548 (1989).

[25] P. Lipa and B. Buschbeck, Phys. Lett. B **223**, 465 (1989).
[26] A. Bialas and R. C. Hwa, Phys. Lett. B **253**, 436 (1991).
[27] A. Bialas and R. Peschanski, Nucl. Phys. **B308**, 803 (1988); A. Bialas and K. Zalewski, Phys. Lett. B **228**, 155 (1989).
[28] R. Peschanski, Nucl. Phys. **B327**, 144 (1989).
[29] H. G. E. Hentschel and I. Procaccia, Physica D **8**, 435 (1983).